THE JOURNAL OF PHYSICAL CHEMISTRY C

Article

pubs.acs.org/JPCC

Control of Symmetry Breaking Size and Aspect Ratio in Gold Nanorods: Underlying Role of Silver Nitrate

Wenming Tong,[†] Michael J. Walsh,[‡] Paul Mulvaney,[∥] Joanne Etheridge,[‡,§] and Alison M. Funston*[,†]

[†]School of Chemistry, [‡]Department of Materials Science and Engineering, and [§]Monash Centre for Electron Microscopy, Monash University, Clayton, Victoria 3800, Australia

[∥]School of Chemistry and Bio21 Institute, University of Melbourne, Parkville, Victoria 3010, Australia

Supporting Information

ABSTRACT: Single crystal gold nanorods remain one of the most important and intensively studied anisotropic nanocrystals. The aspect ratio of the nanorods is controlled during the colloidal synthesis using silver nitrate; however, the mechanisms for the underlying control are not well understood. Here, we investigate the growth of gold nanocrystals at the stage where they break symmetry and begin anisotropic growth into nanorods. Using high resolution electron microscopy, we determine directly the size and atomic structure of the nanocrystals at the symmetry breaking point. We find that silver nitrate controls the size of the crystal at which symmetry breaking occurs. The seed crystal undergoes a symmetry breaking event at a critical diameter between 4 and 6 nm that depends upon the $[HAuCl_4]$:$[AgNO_3]$ ratio. The smallest diameter for symmetry breaking, ∼4 nm, is observed at the lowest $[HAuCl_4]$:$[AgNO_3]$ ratio (i.e., the highest $AgNO_3$ concentration) corresponding to the minimum size at which a "truncation" can form, a precursor to a {110} facet. The diameter of the nanocrystal at the symmetry breaking point becomes the width of the nascent nanorod, and this in turn determines the final nanorod width. Surprisingly, the $[HAuCl_4]$:$[AgNO_3]$ ratio has little effect on the final nanorod length. Our observations explain why the nanorod aspect ratio is constrained within a limited range. This provides a rational framework for controlling width and aspect ratio in the growth of single crystal gold nanorods.

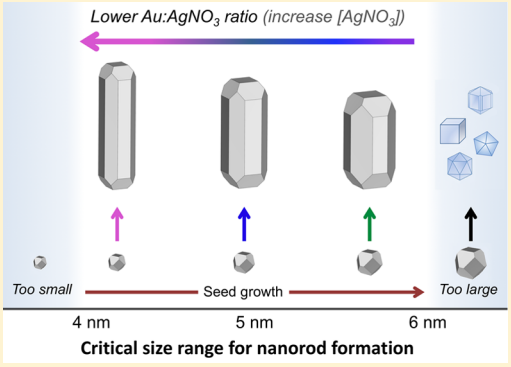

INTRODUCTION

Realizing full control of nanocrystal size and shape is critical for the engineering of functional structures from crystalline nanoparticles. Synthetic methods to grow anisotropic nanocrystals have been developed largely empirically.[1−3] These studies have revealed that the structure of the seed nanocrystal is critical, and that surfactants and adsorbates can promote the formation of different nanocrystalline facets.[1−4] Surfactants may act by altering the effective surface free energy of individual facets (thermodynamic control) or by blocking crystal facets and retarding growth of those facets (kinetic control).[1,5,6] Exploitation of these underpinning principles has enabled the growth of highly anisotropic shapes.[2,7−9]

Gold nanorods are one of the most intensively studied metal nanoparticle systems. The tunability of the rod aspect ratio[7] and therefore optical spectra, along with the strong near-field enhancement at the nanorod tips,[10,11] make them promising candidates for optoelectronic and sensing applications. Gold nanorods with two different morphologies have been synthesized. In the absence of silver ions, decahedral gold nuclei comprising {111} planes grow as rods in the presence of cetyltrimethylammonium bromide (CTAB) with relatively low yields achieved.[8,12,13] In the presence of both silver nitrate and CTAB, the seeds grow into single crystal, rod-shaped particles with a high yield of rods compared to spheres, although only ∼15% of the gold salt is converted into gold metal.[14] The synthetic method for single crystal gold nanorods results in perhaps the highest yield of the desired nanocrystal shape of any anisotropic synthesis, and their growth necessarily requires a lowering of the nanoparticle symmetry.[7,15] For these reasons, single crystal gold nanorods represent the archetypal system for studies of shape control.

For a standard single crystal gold nanorod synthesis,[7] it is well-known that, by gradually increasing the silver nitrate concentration in the growth solution, aspect ratios from 2 up to 4.5 can be achieved, corresponding to longitudinal plasmon resonance wavelengths from 580 nm up to approximately 850 nm.[7] However, further increasing the silver nitrate concentration no longer increases the aspect ratio,[7] and this in turn restricts how far the surface plasmon resonance can be tuned into the infrared regime. The fundamental factors underpinning aspect ratio control are not yet understood. Furthermore, it is unclear whether silver nitrate is involved in just the symmetry breaking step or whether it also influences the subsequent nanorod growth. A complete understanding of these effects is needed if full shape control of nanomaterials is to be achieved.

Received: October 13, 2016
Revised: January 5, 2017
Published: February 2, 2017

DOI: 10.1021/acs.jpcc.6b10343
J. Phys. Chem. C 2017, 121, 3549−3559

Gold nanocrystals of various shapes can be synthesized through careful control of growth kinetics and/or surface selective passivation.[16−18] There have been three different general mechanisms proposed for the growth of gold nanorods: (1) silver underpotential deposition (UPD), in which a monolayer quantity of Ag(0) is proposed to preferentially deposit onto the growing longitudinal facets to favor anisotropic growth;[19] (2) surfactant templating, where elongated CTAB micelles form a soft template for the growth of gold nanorods, potentially with the synergistic involvement of silver in the micelles;[13,20,21] (3) facet-specific capping, where CTA−Br−Ag^+ complexes act as capping agents to block specific facets for anisotropic growth.[22−24] All three models are supported to a certain extent by the experimental data, although none is able to completely explain all experimental observations and there remains considerable debate in the literature regarding the mechanism.[25,26]

During the synthesis of gold nanorods, anisotropic crystal growth from single crystal seeds begins at the very early stages of growth. The rod shape is formed when the particle is at around 5% of its final volume.[19] The synthesis of nanorods has been categorized into five stages.[20] Of these stages, it is proposed that symmetry breaking occurs between stage I and stage II, and further growth following symmetry breaking occurs in stages III−V. In stage I, the cuboctahedral seeds grow isotropically to larger cuboctahedral particles up to a size of ∼6 nm.[20] These larger particles undergo rapid anisotropic growth in stage II while maintaining a diameter of ∼6 nm.[20] The key features of this model are supported by results from in-depth statistical analysis of the size profiles of final nanorod samples for a seedless synthesis of single crystal gold nanorods.[27] The analysis identified a "bifurcation" point at a seed diameter of ∼5 nm,[27] consistent with the critical symmetry breaking size.[28] It was proposed that only those seeds which had broken symmetry prior to achieving the critical size formed nanorods, while those that did not proceeded to form larger more spherical products via a competitive route.[27]

Direct observations of nascent nanorods close to and at the symmetry breaking point have revealed that symmetry breaking of single crystal seeds only occurs in the presence of silver nitrate, and that there are small and asymmetric truncating surfaces with an open atomic structure at the intersection of {111} facets on the small particles.[28] The open atomic structure of the nascent {110} "truncations" is more favorable for silver atom deposition, compared to the denser structure of the lower index facets.[19,28,29] It has been proposed that the truncations may develop into the side facets of the embryonic nanorod structure.[28] Taken together, these factors may explain the concurrent observation of the formation of nascent {110} or higher index "facets" and the onset of symmetry breaking;[28] however, they do not explain the observed aspect ratio control with silver nitrate concentration.

We propose here that silver nitrate primarily exerts control of the nanorod aspect ratio at the symmetry breaking point. To validate this hypothesis, we present a systematic investigation of the role of silver nitrate at the point of symmetry breaking and during subsequent growth, undertaken with extensive high resolution transmission electron microscopy (HRTEM) analysis. The results clearly elucidate the relationships between the concentration of silver nitrate, the size of the seed at the symmetry breaking step, and the final width, length, and aspect ratio of the resultant gold nanorods.

EXPERIMENTAL METHODS

Chemicals. Gold(III) chloride trihydrate ($HAuCl_4·3H_2O$) (≥99.9%), silver nitrate ($AgNO_3$) (≥99.0%), sodium borohydride ($NaBH_4$) (≥99.0%), and L-ascorbic acid (AA) (≥99.0%) were purchased from Sigma-Aldrich. Hexadecyltrimethylammonium bromide (CTAB) (98%) was purchased from Ajax Finechem. All chemicals were used without further purification. Ultrapure water (Milli-Q, R > 18.2 MΩ·cm) was used for the preparation of all solutions.

Synthesis. *Gold Seeds.* An aqueous solution of $HAuCl_4$ (0.025 mL, 0.050 M) was added to an aqueous solution of CTAB (4.70 mL, 0.10 M). The solution was stirred for at least 5 min. Upon rapid addition of freshly prepared $NaBH_4$ (0.30 mL, 0.025 M, at room temperature in ultrapure water) into the solution under vigorous stirring, the initially yellow-orange color became light brown. The resultant dispersion was stirred for 15 min. The final seed dispersion was kept at 29 ± 1 °C in a thermostated water bath for at least 40 min before further use.

Growth of Gold Nanorods from Gold Seeds. An aqueous solution of $HAuCl_4$ (0.10 mL, 0.050 M) was added into an aqueous solution of CTAB (10 mL, 0.10 M). The solution was stirred for at least 5 min. Aqueous solutions of freshly prepared ascorbic acid (0.0552 mL, 0.10 M) and $AgNO_3$ (0.020, 0.040, 0.060, 0.080, or 0.100 mL, 0.010 M) were then added sequentially with thorough mixing following each addition. Finally, an aliquot of the gold seed dispersion (0.012 mL) was added with stirring. The solution gradually changed color from clear to purple/blue over 15 min for lower silver concentrations, and to light pink for higher silver concentrations. The final dispersion was held at 29 ± 1 °C in a thermostated water bath for 2 h.

Overgrowth of Gold Seeds. Aqueous solutions of CTAB (1.50 mL, 0.10 M), Milli-Q water (10.00 mL), and $HAuCl_4$ (0.020 mL, 0.050 M) were mixed and allowed to stir for at least 5 min. An aqueous solution of freshly prepared ascorbic acid (0.020 mL, 0.10 M) was then added and, following complete mixing, the solution color changed from yellow to colorless. Aqueous $AgNO_3$ solution (0, 0.004, 0.008, 0.012, 0.016, or 0.020 mL, 0.010 M) was then added. Finally, the gold seed dispersion (1.00 mL) was added to the above mixture under stirring. The solution became colored within 10 s. The resultant dispersion was grown at 29 ± 1 °C in a thermostated water bath for 30 min.

Growth of Gold Nanorods from Overgrown Seeds. Aqueous solutions of CTAB (10.00 mL, 0.10 M) and $HAuCl_4$ (0.10 mL, 0.050 M) solutions were mixed and allowed to stir for at least 5 min. An aqueous solution of freshly prepared ascorbic acid (0.0552 mL, 0.10 M) was then added, and following complete mixing the solution color changed from yellow to colorless. Aqueous $AgNO_3$ (0, 0.020, 0.040, 0.060, 0.080, or 0.10 mL, 0.010 M) was then added. Finally, the overgrown seed solution (0.120 mL) was added under stirring. The $[HAuCl_4]$:$[AgNO_3]$ ratio employed for each growth solution was matched to that used for the synthesis of the overgrown seeds. The dispersion became colored within 2 min. The resultant nanorod dispersion was grown at 29 ± 1 °C in a thermostated water bath for 2 h.

Timed Addition of Extra Silver Nitrate during Nanorod Growth. An aqueous solution of $HAuCl_4$ (0.10 mL, 0.050 M) was added into an aqueous solution of CTAB (10 mL, 0.10 M). The solution was stirred for at least 5 min. Aqueous solutions of freshly prepared ascorbic acid (0.0552 mL, 0.10 M) and $AgNO_3$

DOI: 10.1021/acs.jpcc.6b10343
J. Phys. Chem. C 2017, 121, 3549−3559

Scheme 1. Schematic Outline of the Synthetic Approaches To Elucidate the Symmetry Breaking Step in the Synthesis of Single Crystal Gold Nanorods[a]

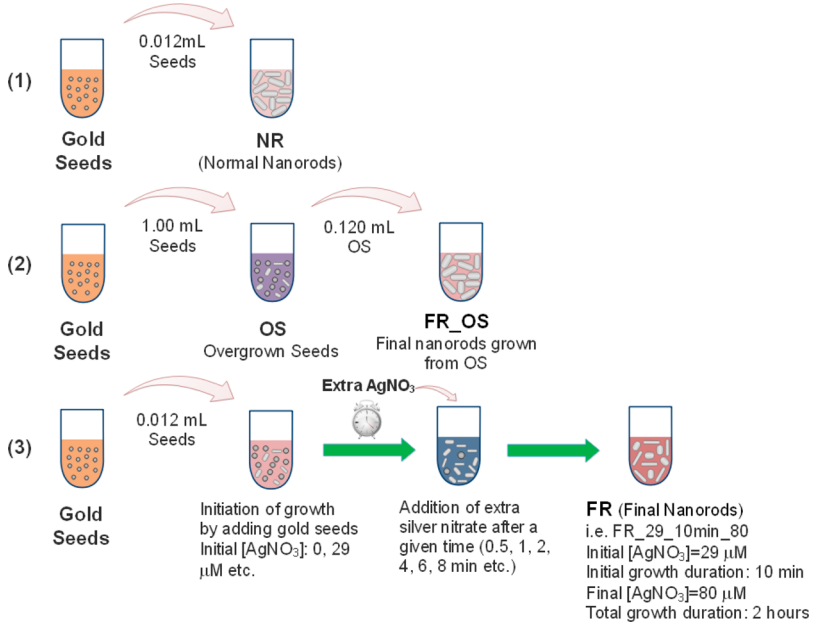

[a](1) Standard seed-mediated growth; (2) gold nanorod growth from overgrown seeds; (3) timed addition of extra silver nitrate during nanorod growth.

(0, 0.010, 0.015, or 0.020 mL, 0.010 M) were then added sequentially with thorough mixing following each addition. Finally, gold seeds (0.012 mL) were added with stirring and the dispersion was held at 29 ± 1 °C in a thermostated water bath. An additional aliquot of $AgNO_3$ (0.080, 0.070, 0.065, or 0.060 mL, 0.010 M) was added at a variable time following the seed addition to bring the total silver concentration to 80 μM. The resultant nanorod dispersion was grown at 29 ± 1 °C in a thermostated water bath to give a total growth time (including time before and after the addition of the silver nitrate aliquot) of 2 h.

Instrumental Techniques. UV−visible extinction spectra were acquired using a Cary 60 UV−vis spectrophotometer or a Cary 5000 UV−vis−NIR spectrophotometer. Extinction spectra were normalized at 400 nm.

Electron microscopy was carried out at the Monash Centre for Electron Microscopy on an FEI Tecnai G2 T20 TWIN TEM and an FEI Titan[3] 80−300 kV FEGTEM fitted with spherical aberration correctors on the probe and image forming lens systems. For overgrown seed particles, all imaging was carried out at 300 kV and at room temperature. Raw data images are shown. Some minor adjustments to contrast and brightness levels were made uniformly across each image.

For the overgrown seeds, following each synthesis, a sample of the overgrowth solution was taken and immediately dropped onto an ultrathin (<3 nm) carbon film supported on a Cu TEM grid for electron microscopic analysis. Fully grown nanorods were centrifuged and redispersed in ultrapure water twice prior to deposition on the TEM grid. Following all sample depositions, the dispersion was allowed to sit (2−5 min) before the TEM grid was soaked in high purity ethanol for ∼20 min to remove excess CTAB. There was then no further treatment of samples prior to electron microscopic analysis.

Samples were labeled according to the codes given in Scheme 1. Nanorods synthesized via the standard seed-mediated growth are labeled according to the convention NR_[$AgNO_3$], where [$AgNO_3$] is the silver nitrate concentration in μM. Overgrown seeds are labeled similarly, i.e. OS_[$AgNO_3$], where [$AgNO_3$] is the silver nitrate concentration in μM. The nanorods grown using overgrown seeds as the seed solution are denoted using FR_[$AgNO_3$]_OS_[$AgNO_3$]. For example, the label FR_80_OS_12.7 indicates the gold nanorods were grown from overgrown seeds containing 12.7 μM silver nitrate concentration, with a silver nitrate concentration of 80 μM in the final nanorod growth solution. Note that, due to the different concentrations of $HAuCl_4$ used in the two steps (see above), the $HAuCl_4$:$AgNO_3$ ratio for both these silver nitrate concentrations is 6.25. For the timed addition of further silver nitrate aliquots, the growth conditions are labeled FR_(initial [$AgNO_3$])_(initial growth duration)_(final [$AgNO_3$]). For example, if the growth is initiated in the presence of 29 μM silver nitrate (upon addition of the gold seed solution), and then extra silver nitrate is added to give a final solution silver nitrate concentration of 80 μM after 10 min of initial growth, the solution is denoted FR_29_10min_80.

RESULTS

The fundamental goal of our research is to identify the primary factors controlling the nanorod aspect ratio and the role of silver nitrate in this process. To do this we identify and characterize the nanorod structure at the symmetry breaking stage at different silver nitrate concentrations to assess the effect of the silver ions at this point. Scheme 1 shows the synthetic approaches employed. The extinction spectra and average length, width, and aspect ratio of the nanorods synthesized via the standard seed-mediated synthesis[7] (row (1)) are shown in Figure S1 and Table S1, respectively, in the Supporting Information. The lowest energy localized surface plasmon resonance (LSPR), the longitudinal resonance, red shifts with increasing silver nitrate concentration, indicative of an increase in aspect ratio.[7,14]

DOI: 10.1021/acs.jpcc.6b10343
J. Phys. Chem. C 2017, 121, 3549−3559

Critical Size for Symmetry Breaking and Effect of the [$HAuCl_4$]:[$AgNO_3$] Ratio. To understand the crucial role of silver ions in the growth of gold nanorods, we have investigated how the silver nitrate concentration present at the symmetry breaking point affects the size, structure, and morphology of the nascent nanorods. The direct observation of nanocrystals at the symmetry breaking stage requires the growth and isolation of gold nanocrystals at this critical point.[28] Subsequently these larger overgrown seeds may be used as seed particles themselves to grow mature gold nanorods (see row (2) of Scheme 1).

The overgrown seeds are synthesized under conditions used for the isotropic overgrowth of gold nanospheres[30] with the exception of the additional silver nitrate. The CTAB concentration used for the seed overgrowth (0.012 M) is lower than that for gold nanorod growth (0.10 M) but well above the critical micelle concentration of CTAB. The [$HAuCl_4$]:[$AgNO_3$] ratio is kept the same in both the overgrowth step and final nanorod growth step. The extinction spectra of the overgrown seed solutions with [$HAuCl_4$]:[$AgNO_3$] ratios of 25 to 5 with a fixed [$HAuCl_4$] of 80 μM are shown in Figure 1a. In the absence of $AgNO_3$, the spectrum

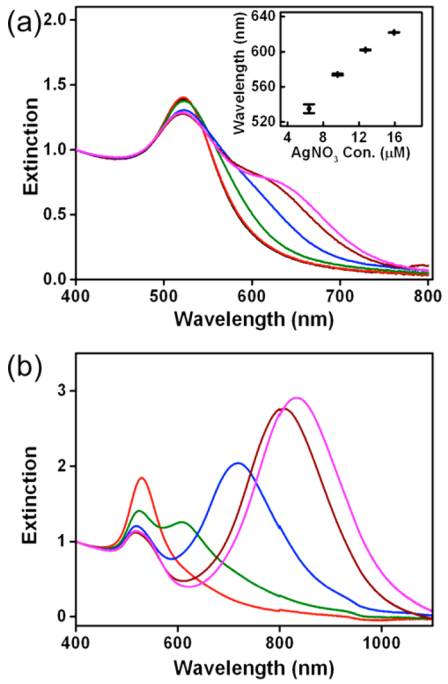

Figure 1. Normalized extinction spectra of (a) overgrown gold seeds in the absence of silver nitrate (black), and with 3.2 (red), 6.4 (olive), 9.6 (blue), 12.7 (wine), and 15.9 μM (magenta) silver nitrate and (b) gold nanorods grown from the overgrown seeds with 20 (red), 39 (olive), 59 (blue), 80 (wine), and 100 μM (magenta) silver nitrate. For both (a) and (b) the [$HAuCl_4$]:[$AgNO_3$] ratios are 25, 12.5, 8.3, 6.25, and 5 in order of increasing silver nitrate concentration. (inset) Lowest energy resonance vs silver nitrate concentration in overgrowth solution (from fits to the sum of two Gaussian functions).

(black line, overlapped with the red line) exhibits a single, symmetric, localized surface plasmon resonance band, characteristic of spherical particles.[30] In the presence of low concentrations of $AgNO_3$ (<10 μM), a broadening of the resonance peaks is seen. Further broadening of the resonance peak is observed for higher $AgNO_3$ concentrations and at the highest concentrations an additional lower energy resonance becomes obvious. Deconvolution of the spectra into two peaks reveals a gradual and approximately linear red shift in the lowest energy plasmon resonance (inset to Figure 1a). This is consistent with the formation of nascent nanorods, at either higher yield or higher average aspect ratio (or both of these) for higher silver nitrate concentration. The extinction spectra obtained upon further growth of the overgrown seeds, in a growth solution with the same [$HAuCl_4$]:[$AgNO_3$] ratio as used for the overgrown seeds, are shown in Figure 1b. The longitudinal band redshifts with increasing concentration of $AgNO_3$ to resemble the spectra of mature gold nanorods observed during the standard growth (Figure S1). This confirms that the nascent nanorods synthesized via the overgrowth can be considered true intermediates in the growth of gold nanorods.

The morphologies and crystal structures of the overgrown seeds are investigated by aberration-corrected phase contrast TEM. The results show that the overgrown seeds are a mixture of spherical and elongated particles as shown in Figure 2. For

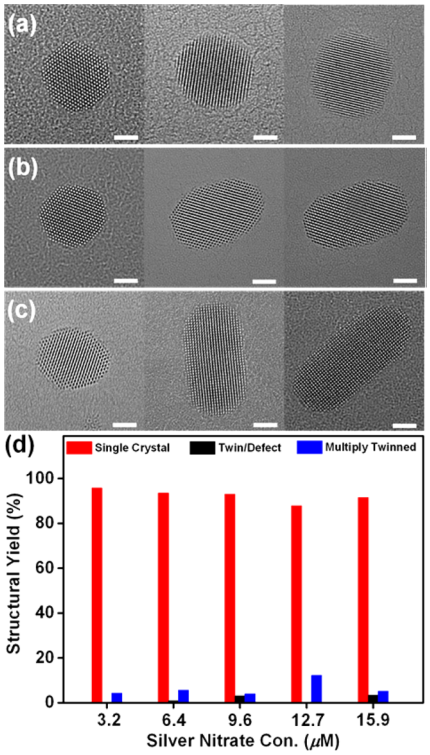

Figure 2. Representative TEM images of overgrown gold seeds with silver nitrate concentrations of (a) 3.2, (b) 9.6, and (c) 15.9 μM in the growth solution and structural yield (d). Other components in overgrowth solutions are [Au] = 80 μM, [ascorbic acid] = 160 μM, [CTAB] = 12 mM, and 1 mL gold seed solution. The scale bars in the images are 2 nm. The breakdown of the numbers of particles analyzed for each sample along with their relative percentages of single crystal, singly twinned and multiply twinned (MTP) particles, as well as the percentage of these that had broken symmetry (AR > 1.25%) are given in the Supporting Information, Table S2.

low concentrations of $AgNO_3$ (Figure 2a), the vast majority of the overgrown seeds maintain their spherical shape. At higher silver nitrate concentrations (Figure 2b,c), a (relatively) higher percentage yield of elongated particles is present (Table S2), exhibiting a range of aspect ratios. Irrespective of the $AgNO_3$ concentration, the yields of single crystal particles for all

DOI: 10.1021/acs.jpcc.6b10343
J. Phys. Chem. C 2017, 121, 3549−3559

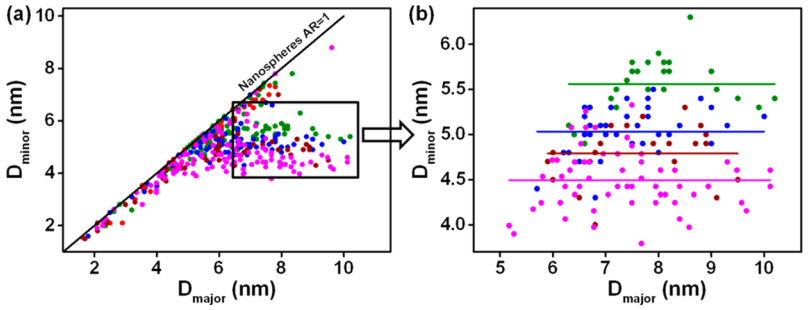

[$AgNO_3$] (μM)	3.2	6.4	9.6	12.7	15.9
Au:$AgNO_3$ (molar)	25	12.5	8.33	6.25	5
Average D_{minor} (nm)	--	5.6 ± 0.3	5.0 ± 0.2	4.8 ± 0.3	4.5 ± 0.3

Figure 3. Size statistics of the overgrown seeds with different concentrations of silver nitrate: 3.2 (red), 6.4 (olive), 9.6 (blue), 12.7 (wine), and 15.9 μM (magenta) with [Au] = 80 μM, [ascorbic acid] = 160 μM, [CTAB] = 12 mM, and 1 mL gold seed solution. (a) Data for all overgrown seeds, (b) data for overgrown seeds with aspect ratio of ≥1.25. The solid line in (a) represents the spherical particles with AR = 1. The solid lines in (b) are the results from the linear fits. The table shows the initial [$HAuCl_4$]:[$AgNO_3$] ratios and average D_{minor}. The percentages of asymmetrically grown particles in overgrown seed samples are given in Table S2.

samples are around 90%. Only a small proportion of particles have twin planes (Figure 2d). Following isotropic growth to the critical size at which symmetry breaking occurs, the particles rapidly elongate with little to no change in their other dimensions, as observed previously.[20] For overgrowth with silver nitrate concentrations higher than 3.2 μM, more than 24% of particles grow anisotropically with an aspect ratio larger than 1.25 (Figure 3 and Table S2). For these nascent crystals, we denote the longer axis D_{major} while the shorter (perpendicular) axis is D_{minor}; the aspect ratio (AR) of the particles is therefore D_{major}/D_{minor}.

The data in Figure 3 reveal that the silver nitrate concentration controls the seed size at which symmetry breaking occurs. Linear extrapolation of D_{minor} at each silver nitrate concentration for which nanocrystals have broken symmetry ($D_{major}/D_{minor} \geq 1.25$) gives the characteristic diameters for symmetry breaking at these silver nitrate concentrations. From these data, it is clear that an increase in silver nitrate concentration causes symmetry breaking at smaller particle diameters. The average value of D_{minor} decreases from 5.6 ± 0.3 to 4.5 ± 0.3 nm as the silver nitrate concentration increases. The characteristic diameters determined for symmetry breaking as a function of silver nitrate concentration are reported in Figure 3. Each of these groups is statistically different (Wilcoxon test with Bonferroni correction, see the Supporting Information for details). At the lowest silver nitrate concentration investigated (3.2 μM), too few particles had broken symmetry to determine a critical size for symmetry breaking. In agreement with previous results, D_{minor} is in the range of 4−6 nm for the majority of the symmetry broken particles at all silver nitrate concentrations investigated here.[28] While D_{minor} has a relatively narrow size distribution, D_{major} has a considerably broader distribution with particle lengths ranging from approximately 6 to 10 nm. A stochastic "popcorn"-like symmetry breaking process has previously been proposed to describe this.[31]

The average width of the final gold nanorods (Table S3) increases as the amount of silver nitrate (or [$HAuCl_4$]:[$AgNO_3$] ratio) decreases. Comparison of this trend with the critical size for symmetry breaking at different silver nitrate concentrations demonstrates that the width of the final nanorods correlates with the symmetry breaking size.

Isolating the role of each additive on the symmetry breaking step is complicated by the fact that the effects of each reagent are highly interrelated.[32,33] Generally, the silver nitrate concentration is changed to control the aspect ratio.[7] However, we find that the same aspect ratio can be obtained by varying the gold ion concentration (keeping the ascorbic acid concentration proportional to this) or by varying the silver ion concentration. It is the [$HAuCl_4$]:[$AgNO_3$] ratio that is critical. Thus, as shown in Figure S2, a comparable longitudinal resonance wavelength tuning to that in Figure S1 can be achieved by varying the gold ion concentration in the nanorod growth. This shows that it is the [$HAuCl_4$]:[$AgNO_3$] ratio, rather than the absolute concentration of silver nitrate, that controls the symmetry breaking point and critical size for the onset of asymmetric growth.

Width and Resultant Aspect Ratio Control by $AgNO_3$. The results from the overgrown seeds presented above clearly establish that the silver nitrate controls the size of the seed at the symmetry breaking point. To clarify how this influences the final nanorod aspect ratio, we modulate the width of nanorods within a colloid by changing the concentration of the silver nitrate during symmetry breaking. The symmetry breaking of an ensemble of nanocrystals in solution is stochastic and occurs over a period of time.[31] Evaluation of the effects of the silver nitrate concentration on the point of symmetry breaking and subsequent growth is therefore achieved by incorporating step changes to the silver nitrate concentration during the symmetry breaking period. This method is schematically illustrated by the lowest pathway in Scheme 1 and allows the introduction of higher silver nitrate concentrations at the different stages of gold nanorod growth. Note that the seeds used to initiate growth in this method are the normal nanorod seeds (they have not been overgrown). The growth conditions in this approach are labeled FR_(initial [$AgNO_3$])_(initial growth duration)_(final [$AgNO_3$]). All solutions in this work are fully described along with the solution code in Table S4.

In the absence of silver nitrate, the seed crystals grow within 6 min to a size which is too large for symmetry breaking to occur. For nanocrystals grown completely in the absence of silver nitrate, the extinction spectrum is indicative of primarily gold nanospheres, i.e. one resonance at 535 nm (black line in Figure 4).[30] A small shoulder resonance is obvious at longer

DOI: 10.1021/acs.jpcc.6b10343
J. Phys. Chem. C 2017, 121, 3549−3559

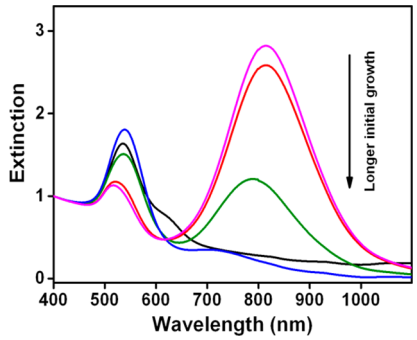

Figure 4. Normalized extinction spectra for the addition of silver nitrate to give a final concentration of 80 μM at different nanorod growth stages, with the growth initiated in the absence of silver nitrate. The initial growth periods are 2 (red), 4 (olive), and 6 min (blue). The spectra of the sample in the absence of silver nitrate (black) and the sample with 80 μM silver nitrate (magenta) are given for comparison.

wavelengths and is likely due to a very low yield of penta-twinned nanorods, known to form under these conditions.[12,34] When silver nitrate is added at different times following the initiation of the growth, the extinction spectra reveal that symmetry breaking (which requires the presence of silver nitrate[28]) occurs only when the silver nitrate is added less than 6 min after growth is initiated. Addition of silver nitrate at times longer than 6 min does not lead to gold nanorod formation as shown by the complete suppression of the longitudinal resonance. Indeed, silver nitrate addition at the 4 min mark following growth initiation already results in a significant decrease in the yield of nanorods (Figure 4), implying that, even at this time point, many of the seeds have grown too large to undergo symmetry breaking. We conclude that symmetry breaking to form nanorods cannot occur once the seeds have grown past a critical size. These results as well as previously reported results[28] give the upper limit to the critical size as ~6–7 nm.

The question therefore arises: if the $[HAuCl_4]$:$[AgNO_3]$ ratio determines the final rod width, what would happen if the ratio is changed during or after the rod symmetry breaking point? Does the reaction pathway change or is the rod aspect ratio fixed? To answer this, we have made step changes to the silver nitrate concentration. Unlike the experiments in Figure 4, here we start with sufficient silver nitrate to initiate rod formation but then add more silver nitrate to see how this influences the final rod morphology. Figure 5a shows extinction

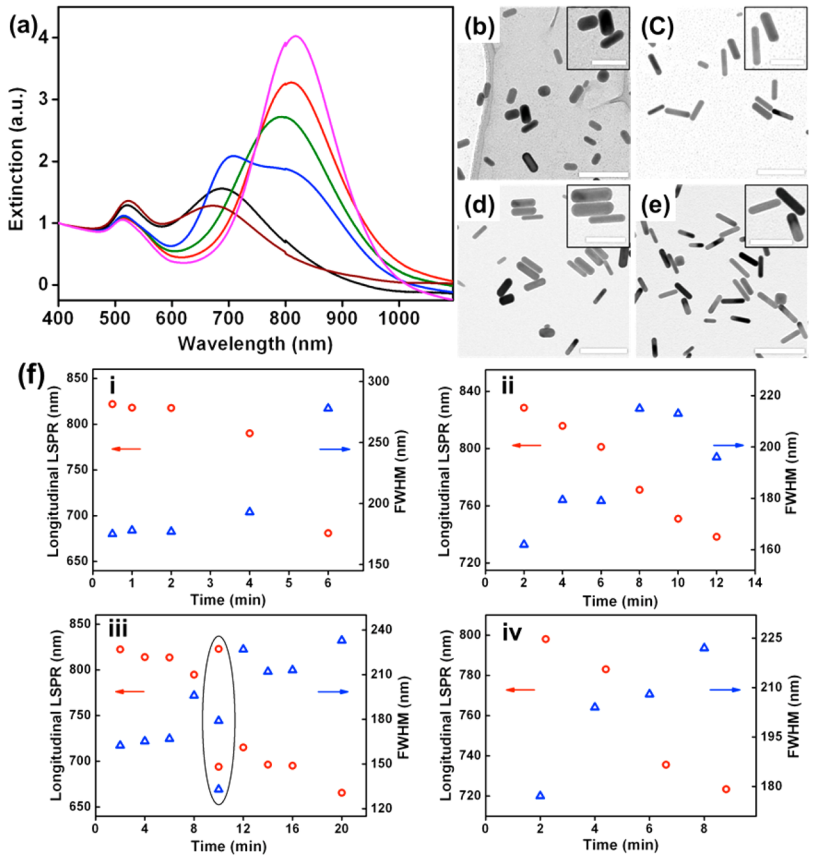

Figure 5. (a) Normalized extinction spectra for the increase in silver nitrate concentration at different nanorod growth stages (initial $[AgNO_3]$ = 29 μM, final $[AgNO_3]$ = 80 μM) and (b–e) selected TEM images of nanorods. The initial growth periods are 6 (red), 8 (green), 10 (blue), and 20 min (wine). The spectra of the nanorods grown with only $[AgNO_3]$ = 29 μM (black) and 80 μM (magenta) are given for comparison. The TEM images are from samples (b) NR_29, (c) FR_29_8min_80, (d) FR_29_10min_80, and (e) NR_80. The scale bars in the TEM images represent 100 nm, while the scale bars in the insets are equal to 50 nm. (f) Relationships between the final longitudinal plasmon band wavelength and the full width at half-maximum (fwhm) as a function of the time prior to the addition of a second silver nitrate aliquot (final $AgNO_3$ = 80 μM). The initial silver nitrate concentrations are (i) 0, (ii) 20, (iii) 29, and (iv) 39 μM. The LSPR positions and fwhm's are obtained by fitting the longitudinal resonance of the spectra to Gaussian curves with an exception for sample FR_29_10min_80 for which the longitudinal resonance peak is deconvoluted into two peaks with two fwhm's (circled area in part f(iii)).

DOI: 10.1021/acs.jpcc.6b10343
J. Phys. Chem. C 2017, 121, 3549–3559

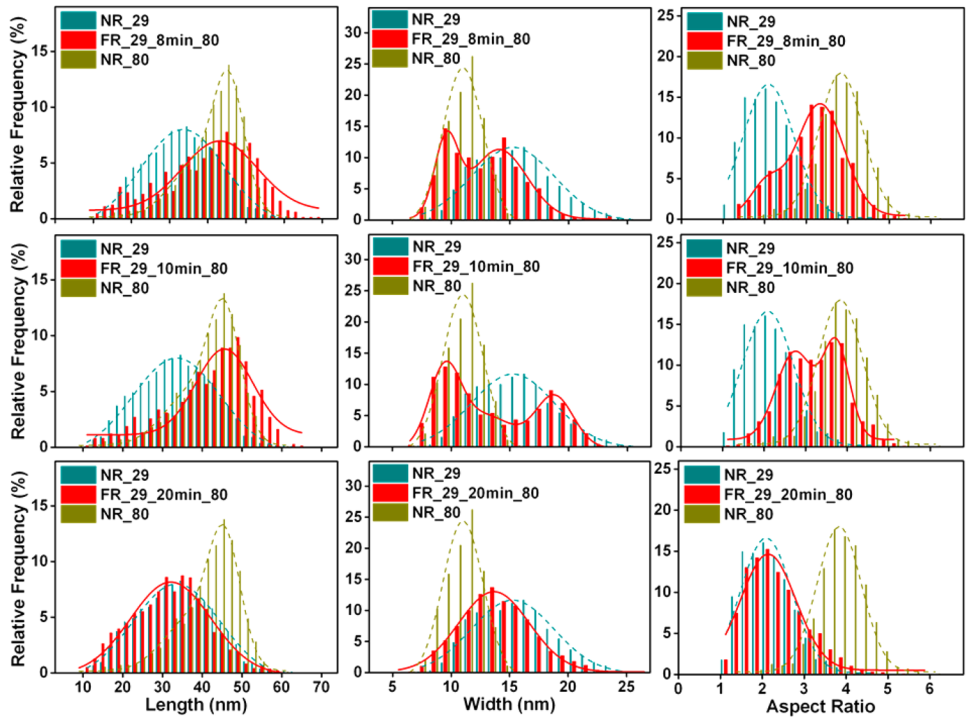

Figure 6. Comparison of statistical analysis on the length, width, and aspect ratios of samples NR_29 (dark cyan), NR_80 (olive), and (top row) FR_29_8min_80 (red), (middle row) FR_29_10min_80 (red), and (bottom row) FR_29_20min_80 (red). Solid and dashed lines are obtained by Gaussian fit. The numbers of particles measured are 3209 for NR_29, 3506 for NR_80, 811 for FR_29_8min_80, 742 for FR_29_10min_80, and 1943 for FR_29_20min_80, respectively.

spectra of the samples from the growth initiated with a low concentration of silver nitrate (29 μM). Addition of extra silver nitrate at times 6 min or earlier results in spectra similar to that of the standard growth with 80 μM silver nitrate (Figure S5). When the initial growth period is 8 min, a distinct reduction in the intensity and broadening of the longitudinal resonance is observed. Similarly, for an initial growth period of 10 min, a splitting of the longitudinal peak into two overlapping peaks is observed, suggestive of two distinct populations with different aspect ratios. The formation of two distinct aspect ratio populations upon addition of excess silver nitrate (at 5 min) has been observed previously.[35] This effect is presumably due to some nanocrystals breaking symmetry under conditions of the lower silver nitrate concentration and others at the higher. Silver nitrate addition at 20 min leads to the extinction spectrum resembling that of gold nanorods grown fully in the lower silver nitrate concentration, 29 μM. This latter result can be explained on the basis that the symmetry breaking has already occurred for the majority of seed particles before 20 min. Similar effects are observed for slightly different initial silver nitrate concentrations (Figures S3–S6).

Gold nanorods synthesized in a growth solution containing a low concentration (29 μM) of silver nitrate are relatively wide and short, with an average width 16 nm, length 34 nm, and aspect ratio 2.2 (Figure 5b and Table S1). Conversely, the nanorods grown in a relatively high silver nitrate concentration (80 μM) are thinner and longer, with an average width of 11 nm, length 38 nm, and therefore aspect ratio 3.5 (Figure 5d and Table S1). When extra silver nitrate is added 8 or 10 min after the initiation of growth with 29 μM silver nitrate (FR_29_8min_80 and FR_29_10min_80 respectively), the TEM images show the presence of both thinner and wider nanorods (Figure 5c and 5d for 8 and 10 min, respectively).

The size statistics for these nanorod samples show that addition of extra silver nitrate during the symmetry breaking step results in a significant change to the width distribution (Figure 6). For FR_29_8min_80, the length (average ~40 nm) of the nanorods is comparable to FR_80 (average ~41 nm). Conversely, the width distribution of the nanorods splits into two populations. One population has an average width of 10 nm while the width of the other population is 14 nm, significantly wider than the nanorods grown fully in the higher concentration of silver nitrate. The latter population has a width distribution more characteristic of nanorods grown in the lower silver nitrate concentration, although with a smaller relative proportion of the largest widths.

Similar trends are apparent for samples grown for 10 min prior to a step change in silver concentration. However, to model the width statistical data satisfactorily for this sample, three Gaussian peaks are required (Figure S7): one for the smaller width (9.5 nm), one for the larger width (19 nm), and an additional, broad Gaussian falling midway between these (13 nm). The length distributions of these products have only one apparent population; therefore, the multiple width distributions map into two distributions in aspect ratio, consistent with the extinction spectra. For FR_29_10min_80, the relative frequency histogram confirms that the wider nanorods give a single population in aspect ratio with mean 2.7, consistent with these being the primary contributing species to the lower aspect ratio population (Figure S8). The length distribution of these wider nanorods is similar to NR_80. Similar to previous reports,[35] addition of the extra silver nitrate at a later time (20 min) (see FR_29_20min_80) results in similar distributions in both length and width and an almost identical aspect ratio distribution to that for sample NR_29, indicating minimal effect of the additional silver nitrate added at this time.

DOI: 10.1021/acs.jpcc.6b10343
J. Phys. Chem. C 2017, 121, 3549−3559

Scheme 2. Control of Nanocrystal Width Populations via Timed Addition of Extra Silver Nitrate[a]

[a]The solutions initially grown for 2 and 20 min were further grown for 118 and 100 min respectively to give a total time of growth of 2 h, and similarly for all solutions initially grown for different periods of initial growth.

Early in the symmetry breaking period, only small numbers of seed particles have reached the symmetry breaking size range (4–6 nm). Addition of silver at this point causes the majority of the seed particles to break symmetry at the size characteristic for the lower $[HAuCl_4]$:$[AgNO_3]$ ratio. Midway through the symmetry breaking period (i.e., 10 min in Figure 5a), two groups of particles are present: those that have grown to the critical size for that particular $[HAuCl_4]$:$[AgNO_3]$ ratio (~5.3 nm) and undergone symmetry breaking with a higher $[HAuCl_4]$:$[AgNO_3]$ ratio, and spherical nanocrystals smaller than this. The former grow to nanorods with a larger width. Addition of extra silver nitrate at this point rapidly decreases the $[HAuCl_4]$:$[AgNO_3]$ ratio in the growth solution and promotes rapid symmetry breaking of the remaining, generally smaller spherical nanocrystals. This somewhat "immediate" symmetry breaking results in final nanorods of smaller width, causing the multiple distributions of width and therefore aspect ratio, as the length distribution is largely unaffected. This is summarized in Scheme 2. This explanation is also consistent with previous observations on the effects of spiking the growth solution with silver nitrate.[35]

For nanocrystal growth in the absence of silver nitrate, the seed particles grow to the critical symmetry breaking size at around 4 min (Figure 4). When the growth is initiated in the presence of silver nitrate, the initial growth occurs more slowly, and the critical symmetry breaking size is reached after 6–12 min of growth (Figure 5a). The reduction in growth rate in the presence of silver nitrate is consistent with previous reports,[36] while the relatively long time period over which symmetry breaking occurs is characteristic of a stochastic growth mechanism.[31] We deduce from these results that both the critical size of the seeds and the time at which symmetry breaking occurs can be modulated by tuning the silver nitrate concentration (or $[AuHCl_4]$:$[AgNO_3]$) at early growth times.

DISCUSSION

We have carried out a systematic study of the effects of the silver nitrate on the formation of gold nanorods from gold seeds and its role in symmetry breaking and control of the aspect ratio. We have undertaken exhaustive TEM studies to follow statistically the size distributions of seeds that grow and evolve into rods under a range of solution conditions. We have focused on the ratio of $[HAuCl_4]$:$[AgNO_3]$ and studied how the time point of silver nitrate addition affects the rod growth process. The key observations from these experiments are as follows:

(i) Symmetry breaking of cuboctahedral seeds occurs within a small size range, approximately 4–6 nm.

(ii) The absolute symmetry breaking size within this range is determined by the $[HAuCl_4]$:$[AgNO_3]$ ratio in the growth solution.

(iii) The diameter of spherical nanocrystals at the symmetry breaking point increases with increasing $[HAuCl_4]$:$[AgNO_3]$ ratio (at constant ascorbic acid and CTAB concentration).

(iv) The absolute size at which symmetry breaking occurs determines the final width of the nanorods and therefore the aspect ratio.

(v) Aspect ratio control by silver nitrate ($[HAuCl_4]$:$[AgNO_3]$) is exerted during the symmetry breaking period.

(vi) The length of the final nanorods formed is dependent upon the available gold atom concentration.

These are summarized in Scheme 3, and we now discuss each of these points in turn.

Scheme 3. Summary of the Effect of Silver Nitrate Concentration on the Critical Crystal Diameter at Which Symmetry Breaking and Subsequent Nanorod Growth Occur and Corresponding Width and Aspect Ratio Control[a]

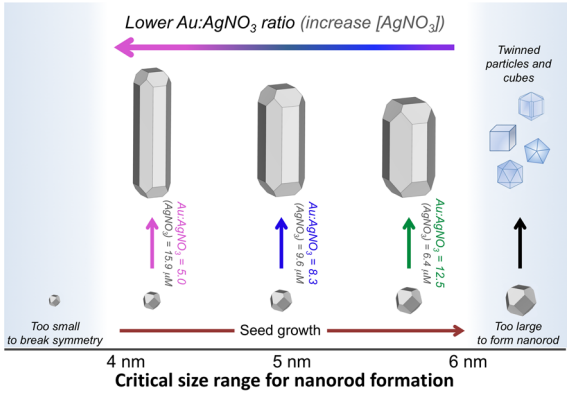

[a]"Au" represents the concentration of gold atoms, given by the initial $[HAuCl_4]$.

(i) Upper and Lower Size Limits. Symmetry breaking occurs between the size limits of ~4 and 6 nm, consistent with previous results.[19,20,27,28] These upper and lower size limits place fundamental constraints on the final aspect ratio that can be achieved. For the *upper size limit*, sensitive structural constraints may play an important role. Growth of the single crystal cuboctahedral seeds beyond ~6 nm in the absence of silver nitrate leads to an increasing proportion of twinned particles.[28] Therefore, isotropic growth of seeds beyond ~6 nm reduces the number of particles with the necessary single crystal structure for growth into single crystal nanorods. It is possible

DOI: 10.1021/acs.jpcc.6b10343
J. Phys. Chem. C 2017, 121, 3549–3559

this upper size limit is slightly larger than 6 nm—we observed very little symmetry breaking at the lowest silver nitrate concentration used here.

The *lower size limit* for symmetry breaking, observed both here and previously, is ∼4 nm.[28] At this size, the emergence of "truncations", i.e. the loss of a few atoms at the intersection of {111} facets, has been reported previously.[28] These truncations mark the onset of formation of nascent {110} facets, which possess a more open atomic structure than either the {111} or {100} surfaces present in perfect cuboctahedra. In the presence of silver nitrate these become more apparent, and have been proposed to grow into the side facets of the nascent nanorods.[28] For smaller particle sizes, the particle surface facets comprise only a few atoms and the creation of higher index truncations to remove undercoordinated edge atoms is unfavorable. This places a fundamental lower limit on the size of particles that may break symmetry. In turn, this imposes a limit on how far the aspect ratio can be increased by the addition of larger concentrations of $AgNO_3$.

(ii, iii) Effect of the [$HAuCl_4$]:[$AgNO_3$] Ratio on the Critical Size for Symmetry Breaking. The absolute size of particle symmetry breaking between the limits outlined above varies as a function of silver nitrate concentration, corresponding to changes in the [$HAuCl_4$]:[$AgNO_3$] ratio. Theoretical studies have shown that, as the particle size decreases, there is an expected underpotential−overpotential deposition transition, placing a lower limit on the particle size at which UPD can occur.[37−39] In the limit of small particle diameters, deposition of silver is increasingly unfavorable due to the increased ratio of edge and corner atoms relative to those within facets.[37,38] The size at which this underpotential−overpotential deposition transition occurs is predicted to be dependent on the particle geometry and system potentials. Accordingly, it may be expected that higher $AgNO_3$ concentrations will result in the onset of silver deposition at smaller particle sizes. This is consistent with the trend in the absolute size of the particles at the symmetry breaking point observed here; that is, symmetry breaking occurs at smaller particle sizes for lower [$HAuCl_4$]:[$AgNO_3$] ratios (i.e. higher silver nitrate concentrations). This lends weight to the involvement of underpotential deposition of silver onto the nanocrystal surface in the mechanism for symmetry breaking.

These results provide further evidence that silver nitrate is a necessary requirement for symmetry breaking. A related and important question then is the role of the CTAB. The Br^- ions are known to bind to the gold surface, and the CTA^+ cations form a bilayer structure over this.[40,41] Silver nitrate, CTA^+, and Br^- (in which the bromide is added as CTAB and/or KBr[36]) slow down the crystal growth. The bromide ion has been implicated as a shape-directing agent,[25,42] and this area has recently been reviewed.[25] However, further elucidation of the mechanism of action of the bromide ion in the symmetry breaking step and further growth of the nanorods is required. Here we show that the [$HAuCl_4$]:[$AgNO_3$] ratio controls the size of the seed at the symmetry breaking point and therefore the aspect ratio of the nanorods. The experimental strategy used here could potentially be exploited to analyze the influence of the bromide ion concentration on the structure and size of the gold seeds at the symmetry breaking step and during further growth.

(iv, v) Absolute Size at Which Symmetry Breaking Occurs Determines the Width of the Gold Nanorods and Therefore Controls the Aspect Ratio. The critical size for symmetry breaking is given by the [$HAuCl_4$]:[$AgNO_3$] ratio. While the nascent rods grow substantially in length, they also increase slightly in width during the growth period. The relative increase in width varies slightly across the different silver nitrate concentrations, such that it is lower in the presence of a higher silver nitrate concentration (Table S2). The discrete size at which symmetry breaking occurs for a given [$HAuCl_4$]:[$AgNO_3$] ratio combined with the characteristic increases in width determines the final widths of the resultant gold nanorods.

The addition of extra silver nitrate (i.e., decreasing [$HAuCl_4$]:[$AgNO_3$] ratio) following symmetry breaking has very limited effect on the final nanorod width. Therefore, the aspect ratio control that is exerted by silver nitrate occurs during the symmetry breaking period, not the subsequent growth stages. This, however, does not preclude the necessity for some silver nitrate to be present to ensure rod-like crystal growth is maintained following symmetry breaking.

(vi) Length of the Final Nanorods. The distribution statistics show (i.e., Figure 6) that the length distribution of the nanorods remains largely unchanged upon addition of excess silver nitrate during the symmetry breaking period. Given the width of the nanorod is fixed at the time of symmetry breaking and allowing for only the slight increase in widths observed during growth, the remaining available gold must be incorporated into the nanorods so as to increase the nanorod length. Previous analysis of the supernatant of gold nanorods following synthesis has shown that, for all silver nitrate concentrations, only ∼15% of the Au^{3+} salt added is incorporated into the rods as Au atoms.[14] This gives a finite length possible for nanorods with a relatively monodisperse gold nanorod sample and a given number of particles. The calculated volumes (V_{rod}) of the gold nanorods are shown in Table S5. Taking into account the concentration of particles in the solutions (N_{rod}) as the accessible gold must be spread across all nanorods, we find that across all silver nitrate concentrations $V_{rod}N_{rod}$ = constant, implying that the nanorod length is limited only by the accessible gold concentration. Narrower nanorods are able to grow longer before the available gold is depleted compared to wider nanorods.

These results explain the previous observations that nanorods synthesized with low silver nitrate concentrations are both wider and shorter, as it requires more gold atoms to increase the length of the nanorod. Conversely, nanorods synthesized at higher silver nitrate concentrations tend to be longer and narrower. The histograms in Figure S8 show that the population of wider nanorods formed during the timed silver nitrate addition (which broke symmetry under conditions of a higher [$HAuCl_4$]:[$AgNO_3$] ratio), has significantly longer nanorods compared to the length of the nanorods grown—with comparable width—without the addition of excess silver (NR_29). The fact that significantly longer nanorods can be grown is evidence that the nanorod length is not fixed at the time of symmetry breaking but depends upon the concentration of accessible gold. This finding suggests that it may be possible to increase the aspect ratio of the single crystal nanorods further by providing more available gold in the solution. In this respect, the timing of the addition of further gold may be critical, and potentially limited by the required [$HAuCl_4$]:[$AgNO_3$] ratio throughout the symmetry breaking period. The intrinsic nanocrystal structure, kinetic constraints, and growth mechanism may also be limiting factors.

DOI: 10.1021/acs.jpcc.6b10343
J. Phys. Chem. C 2017, 121, 3549−3559

CONCLUSIONS

The critical sizes for symmetry breaking of precursor cuboctahedral nanocrystals to form nanorods depends directly on the $[HAuCl_4]$:$[AgNO_3]$ ratio, but always occurs within the size range of 4−6 nm. The nanocrystals break symmetry at progressively smaller sizes for lower $[HAuCl_4]$:$[AgNO_3]$ ratios. The diameter of the nanocrystal at the symmetry breaking point determines the final width of the gold nanorods. The length of the nanoparticles formed is dictated by the available gold concentration, nanorod width, and number of growing particles. The combined outcome of these factors results in the observed control of the nanoparticle aspect ratio with $[HAuCl_4]$:$[AgNO_3]$ ratio. The major influence of silver nitrate on the aspect ratio effectively occurs at the point of symmetry breaking. These results identify the critical role of silver nitrate in breaking the symmetry of isotropic gold seeds and, in turn, on the final width and aspect ratio of the gold nanorods.

ASSOCIATED CONTENT

Supporting Information

The Supporting Information is available free of charge on the ACS Publications Web site. The Supporting Information is available free of charge on the ACS Publications website at DOI: 10.1021/acs.jpcc.6b10343.

Detailed sample descriptions, result for Wilcoxon test with Bonferroni correction, UV−vis extinction spectra for standard gold nanorods and gold nanorods with step-change additions of silver nitrate, size statistics of gold nanorods, and size distributions of gold nanorods (PDF)

AUTHOR INFORMATION

Corresponding Author

*E-mail: alison.funston@monash.edu.

ORCID

Paul Mulvaney: 0000-0002-8007-3247

Alison M. Funston: 0000-0002-4320-6434

Notes

The authors declare no competing financial interest.

ACKNOWLEDGMENTS

This work was supported by the Australian Research Council (ARC) Grants DP120101573 and DP160104679 and used microscopes at the Monash Centre for Electron Microscopy funded by ARC Grant LE0454166. A.M.F. acknowledges the ARC support through the Future fellowship funding (FT110100545). P.M. thanks the ARC for support through FL100100117. W.T. thanks the Australian Government (Department of Education and Training) and Monash University for providing scholarships (IPRS and APA). The authors wish to express their sincere thanks to Dr. Laurent Lermusiaux for his assistance in manuscript preparation.

REFERENCES

(1) Xia, Y.; Xia, X.; Peng, H.-C. Shape-Controlled Synthesis of Colloidal Metal Nanocrystals: Thermodynamic versus Kinetic Products. *J. Am. Chem. Soc.* **2015**, *137*, 7947−7966.

(2) Grzelczak, M.; Pérez-Juste, J.; Mulvaney, P.; Liz-Marzán, L. M. Shape Control in Gold Nanoparticle Synthesis. *Chem. Soc. Rev.* **2008**, *37*, 1783.

(3) Lohse, S. E.; Murphy, C. J. The Quest for Shape Control: A History of Gold Nanorod Synthesis. *Chem. Mater.* **2013**, *25*, 1250−1261.

(4) Katz-Boon, H.; Rossouw, C. J.; Weyland, M.; Funston, A. M.; Mulvaney, P.; Etheridge, J. Three-Dimensional Morphology and Crystallography of Gold Nanorods. *Nano Lett.* **2011**, *11*, 273−278.

(5) Katz-Boon, H.; Walsh, M.; Dwyer, C.; Mulvaney, P.; Funston, A. M.; Etheridge, J. Stability of Crystal Facets in Gold Nanorods. *Nano Lett.* **2015**, *15*, 1635−1641.

(6) Almora-Barrios, N.; Novell-Leruth, G.; Whiting, P.; Liz-Marzán, L. M.; López, N. Theoretical Description of the Role of Halides, Silver, and Surfactants on the Structure of Gold Nanorods. *Nano Lett.* **2014**, *14*, 871−875.

(7) Nikoobakht, B.; El-Sayed, M. A. Preparation and Growth Mechanism of Gold Nanorods (NRs) Using Seed-Mediated Growth Method. *Chem. Mater.* **2003**, *15*, 1957−1962.

(8) Jana, N. R.; Gearheart, L.; Murphy, C. J. Seed-Mediated Growth Approach for Shape-Controlled Synthesis of Spheroidal and Rod-like Gold Nanoparticles Using a Surfactant Template. *Adv. Mater.* **2001**, *13*, 1389−1393.

(9) Personick, M. L.; Mirkin, C. A. Making Sense of the Mayhem Behind Shape Control in the Synthesis of Gold Nanoparticles. *J. Am. Chem. Soc.* **2013**, *135*, 18238−18247.

(10) Funston, A. M.; Novo, C.; Davis, T. J.; Mulvaney, P. Plasmon Coupling of Gold Nanorods at Short Distances and in Different Geometries. *Nano Lett.* **2009**, *9*, 1651−1658.

(11) Aizpurua, J.; Bryant, G. W.; Richter, L. J.; García de Abajo, F. J.; Kelley, B. K.; Mallouk, T. Optical Properties of Coupled Metallic Nanorods for Field-Enhanced Spectroscopy. *Phys. Rev. B: Condens. Matter Mater. Phys.* **2005**, *71*, 235420.

(12) Jana, N. R.; Gearheart, L.; Murphy, C. J. Wet Chemical Synthesis of High Aspect Ratio Cylindrical Gold Nanorods. *J. Phys. Chem. B* **2001**, *105*, 4065−4067.

(13) Jana, N. R. Gram-Scale Synthesis of Soluble, Near-Monodisperse Gold Nanorods and Other Anisotropic Nanoparticles. *Small* **2005**, *1*, 875−882.

(14) Orendorff, C. J.; Murphy, C. J. Quantitation of Metal Content in the Silver-Assisted Growth of Gold Nanorods. *J. Phys. Chem. B* **2006**, *110*, 3990−3994.

(15) Vigderman, L.; Zubarev, E. R. High-Yield Synthesis of Gold Nanorods with Longitudinal SPR Peak Greater than 1200 Nm Using Hydroquinone as a Reducing Agent. *Chem. Mater.* **2013**, *25*, 1450−1457.

(16) Personick, M. L.; Langille, M. R.; Zhang, J.; Mirkin, C. A. Shape Control of Gold Nanoparticles by Silver Underpotential Deposition. *Nano Lett.* **2011**, *11*, 3394−3398.

(17) Langille, M. R.; Personick, M. L.; Zhang, J.; Mirkin, C. A. Defining Rules for the Shape Evolution of Gold Nanoparticles. *J. Am. Chem. Soc.* **2012**, *134*, 14542−14554.

(18) Personick, M. L.; Langille, M. R.; Wu, J.; Mirkin, C. A. Synthesis of Gold Hexagonal Bipyramids Directed by Planar-Twinned Silver Triangular Nanoprisms. *J. Am. Chem. Soc.* **2013**, *135*, 3800−3803.

(19) Liu, M. Z.; Guyot-Sionnest, P. Mechanism of Silver(I)-Assisted Growth of Gold Nanorods and Bipyramids. *J. Phys. Chem. B* **2005**, *109*, 22192−22200.

(20) Park, K.; Drummy, L. F.; Wadams, R. C.; Koerner, H.; Nepal, D.; Fabris, L.; Vaia, R. A. Growth Mechanism of Gold Nanorods. *Chem. Mater.* **2013**, *25*, 555−563.

(21) Wadams, R. C.; Fabris, L.; Vaia, R. A.; Park, K. Time-Dependent Susceptibility of the Growth of Gold Nanorods to the Addition of a Cosurfactant. *Chem. Mater.* **2013**, *25*, 4772−4780.

(22) Hubert, F.; Testard, F.; Spalla, O. Cetyltrimethylammonium Bromide Silver Bromide Complex as the Capping Agent of Gold Nanorods. *Langmuir* **2008**, *24*, 9219−9222.

(23) Almora-Barrios, N.; Novell-Leruth, G.; Whiting, P.; Liz-Marzán, L. M.; López, N. Theoretical Description of the Role of Halides, Silver, and Surfactants on the Structure of Gold Nanorods. *Nano Lett.* **2014**, *14*, 871−875.

(24) Niidome, Y.; Nakamura, Y.; Honda, K.; Akiyama, Y.; Nishioka, K.; Kawasaki, H.; Nakashima, N. Characterization of Silver Ions Adsorbed on Gold Nanorods: Surface Analysis by Using Surface-

Assisted Laser Desorption/Ionization Time-of-Flight Mass Spectrometry. *Chem. Commun.* **2009**, 1754.
(25) Lohse, S. E.; Burrows, N. D.; Scarabelli, L.; Liz-Marzán, L. M.; Murphy, C. J. Anisotropic Noble Metal Nanocrystal Growth: The Role of Halides. *Chem. Mater.* **2014**, *26*, 34−43.
(26) Burrows, N. D.; Harvey, S.; Idesis, F. A.; Murphy, C. J. Understanding the Seed-Mediated Growth of Gold Nanorods through a Fractional Factorial Design of Experiments. *Langmuir* **2016**, DOI: 10.1021/acs.langmuir.6b03606.
(27) Hubert, F.; Testard, F.; Rizza, G.; Spalla, O. Nanorods versus Nanospheres: A Bifurcation Mechanism Revealed by Principal Component TEM Analysis. *Langmuir* **2010**, *26*, 6887−6891.
(28) Walsh, M. J.; Barrow, S. J.; Tong, W.; Funston, A. M.; Etheridge, J. Symmetry Breaking and Silver in Gold Nanorod Growth. *ACS Nano* **2015**, *9*, 715−724.
(29) Jha, K. C.; Liu, H.; Bockstaller, M. R.; Heinz, H. Facet Recognition and Molecular Ordering of Ionic Liquids on Metal Surfaces. *J. Phys. Chem. C* **2013**, *117*, 25969−25981.
(30) Rodríguez-Fernández, J.; Pérez-Juste, J.; García de Abajo, F. J.; Liz-Marzán, L. M. Seeded Growth of Submicron Au Colloids with Quadrupole Plasmon Resonance Modes. *Langmuir* **2006**, *22*, 7007−7010.
(31) Edgar, J. A.; McDonagh, A. M.; Cortie, M. B. Formation of Gold Nanorods by a Stochastic "Popcorn" Mechanism. *ACS Nano* **2012**, *6*, 1116−1125.
(32) Sau, T. K.; Murphy, C. J. Seeded High Yield Synthesis of Short Au Nanorods in Aqueous Solution. *Langmuir* **2004**, *20*, 6414−6420.
(33) Sau, T. K.; Murphy, C. J. Room Temperature, High-Yield Synthesis of Multiple Shapes of Gold Nanoparticles in Aqueous Solution. *J. Am. Chem. Soc.* **2004**, *126*, 8648−8649.
(34) Pérez-Juste, J.; Liz-Marzán, L. M.; Carnie, S.; Chan, D. Y. C.; Mulvaney, P. Electric-Field-Directed Growth of Gold Nanorods in Aqueous Surfactant Solutions. *Adv. Funct. Mater.* **2004**, *14*, 571−579.
(35) Yang, J. A.; Lohse, S. E.; Boulos, S. P.; Murphy, C. J. The Early Life of Gold Nanorods: Temporal Separation of Anisotropic and Isotropic Growth Modes. *J. Cluster Sci.* **2012**, *23*, 799−809.
(36) Bullen, C.; Zijlstra, P.; Bakker, E.; Gu, M.; Raston, C. Chemical Kinetics of Gold Nanorod Growth in Aqueous CTAB Solutions. *Cryst. Growth Des.* **2011**, *11*, 3375−3380.
(37) Oviedo, O. A.; Reinaudi, L.; Leiva, E. P. M. The Limits of Underpotential Deposition in the Nanoscale. *Electrochem. Commun.* **2012**, *21*, 14−17.
(38) Oviedo, O. A.; Vélez, P.; Macagno, V. A.; Leiva, E. P. M. Underpotential Deposition: From Planar Surfaces to Nanoparticles. *Surf. Sci.* **2015**, *631*, 23−34.
(39) Mariscal, M. M.; Oviedo, O. A.; Leiva, E. P. M. On the Selective Decoration of Facets in Metallic Nanoparticles. *J. Mater. Res.* **2012**, *27*, 1777−1786.
(40) Lee, S.; Anderson, L. J. E.; Payne, C. M.; Hafner, J. H. Structural Transition in the Surfactant Layer that Surrounds Gold Nanorods as Observed by Analytical Surface-Enhanced Raman Spectroscopy. *Langmuir* **2011**, *27*, 14748−14756.
(41) Nikoobakht, B.; El-Sayed, M. A. Evidence for Bilayer Assembly of Cationic Surfactants on the Surface of Gold Nanorods. *Langmuir* **2001**, *17*, 6368−6374.
(42) Garg, N.; Scholl, C.; Mohanty, A.; Jin, R. The Role of Bromide Ions in Seeding Growth of Au Nanorods. *Langmuir* **2010**, *26*, 10271−10276.

DOI: 10.1021/acs.jpcc.6b10343
J. Phys. Chem. C 2017, 121, 3549−3559